

This is an Open Access document downloaded from ORCA, Cardiff University's institutional repository: <https://orca.cardiff.ac.uk/id/eprint/42170/>

This is the author's version of a work that was submitted to / accepted for publication.

Citation for final published version:

Wu, Jing , Martin, Ralph Robert, Rosin, Paul L. , Sun, Xianfang , Langbein, Frank Curd , Lai, Yukun , Marshall, Andrew David and Liu, Y.- H. 2013. Making bas-reliefs from photographs of human faces. *Computer-Aided Design* 45 (3) , pp. 671-682. 10.1016/j.cad.2012.11.002

Publishers page: <http://dx.doi.org/10.1016/j.cad.2012.11.002>

Please note:

Changes made as a result of publishing processes such as copy-editing, formatting and page numbers may not be reflected in this version. For the definitive version of this publication, please refer to the published source. You are advised to consult the publisher's version if you wish to cite this paper.

This version is being made available in accordance with publisher policies. See <http://orca.cf.ac.uk/policies.html> for usage policies. Copyright and moral rights for publications made available in ORCA are retained by the copyright holders.



# Making Bas-reliefs from Photographs of Human Faces

J. Wu, R.R. Martin, P.L. Rosin, X.-F. Sun, F.C. Langbein, Y.-K. Lai,  
A.D. Marshall<sup>a</sup>, Y.-H. Liu<sup>b</sup>

<sup>a</sup>*School of Computer Science & Informatics, Cardiff University, Cardiff CF24 3AA, UK*

<sup>b</sup>*Department of Computer Science, Aberystwyth University, Aberystwyth SY23 3DB, UK*

---

## Abstract

Bas-reliefs are a form of flattened artwork, part-way between 3D sculpture and 2D painting. Recent research has considered automatic bas-relief generation from 3D scenes. However, little work has addressed the generation of bas-reliefs from 2D images. In this paper, we propose a method to automatically generate bas-relief surfaces from frontal photographs of human faces, with potential applications to e.g. coinage and commemorative medals.

Our method has two steps. Starting from a photograph of a human face, we first generate a plausible *image* of a bas-relief of the same face. Secondly, we apply shape-from-shading to this generated bas-relief image to determine the 3D shape of the final bas-relief. To model the mapping from an input photograph to the image of a corresponding bas-relief, we use a feedforward network. The training data comprises images generated from an input 3D model of a face, and images generated from a corresponding bas-relief; the latter is produced by an existing 3D model-to-bas-relief algorithm. A saliency map of the face controls both model building, and bas-relief generation.

Our experimental results demonstrate that the generated bas-relief surfaces are smooth and plausible, with correct global geometric nature, the latter giving them a stable appearance under changes of viewing direction and illumination.

## *Keywords:*

Bas-relief, photograph, feedforward network, image relighting, shape from shading

---

*Email addresses:* {J.Wu, ralph, paul, Xianfang.Sun, F.C.Langbein, Yukun.Lai, dave}@cs.cardiff.ac.uk (J. Wu, R.R. Martin, P.L. Rosin, X.-F. Sun, F.C. Langbein, Y.-K. Lai, A.D. Marshall), yy1@aber.ac.uk (Y.-H. Liu)

---

## 1. Introduction

Bas-reliefs are a form of flattened sculpture applied to a base surface. Compared to high-reliefs, bas-reliefs have a limited height above the background, and no part is undercut. They can be considered to be part way between sculpture and painting. Bas-reliefs have been used for centuries in art and architectural decoration, for example as portraits on coins. In modern times, they are also popular in industrial design, for example for branding packaging. However, the production of bas-reliefs requires considerable artistic skill and manual effort. In the fields of computer aided design and computer graphics, recent research [1, 2, 3, 4, 5, 6] has considered automatic bas-relief generation from *3D scenes*. However, as such methods are based on 3D input data, this restricts their range of application, as the necessary 3D input models require specialised and expensive equipment for capture, or must be created laboriously by hand. An alternative approach, with potentially much wider application, is to generate bas-reliefs from *2D images*. However, little work has addressed this problem [7, 8].

Here, we consider a specific problem: the production of a bas-relief from a single frontal photograph of a human face. We focus on human faces, since the face is of special interest in bas-reliefs, especially for coinage and commemorative medals. We mainly address frontal faces here as they are somewhat simpler to process, even though applications often also use profile or semi-profile views. Frontal faces have fixed head pose, and eliminate the necessity of head pose estimation for face images with semi-profile views. Moreover, many frontal face databases exist, facilitating experiments, for example on image relighting. Nevertheless, as we do not use any specific attributes of frontal faces (such as symmetry), our method can in principle be extended to other views. Indeed, our experiments, demonstrate an example using a non-frontal face too.

Our approach is based on shape-from-shading (SFS) [9, 10, 11], a standard technique to recover 3D shape from a single image of an object, based on a model of variation of reflected intensities as a function of surface orientation. However, generating a bas-relief surface from a human face image is not straightforward. One approach would be to use SFS to directly recover the 3D shape of the face as a depth map, and then process that with one of the existing bas-relief production algorithms given above. We do not take

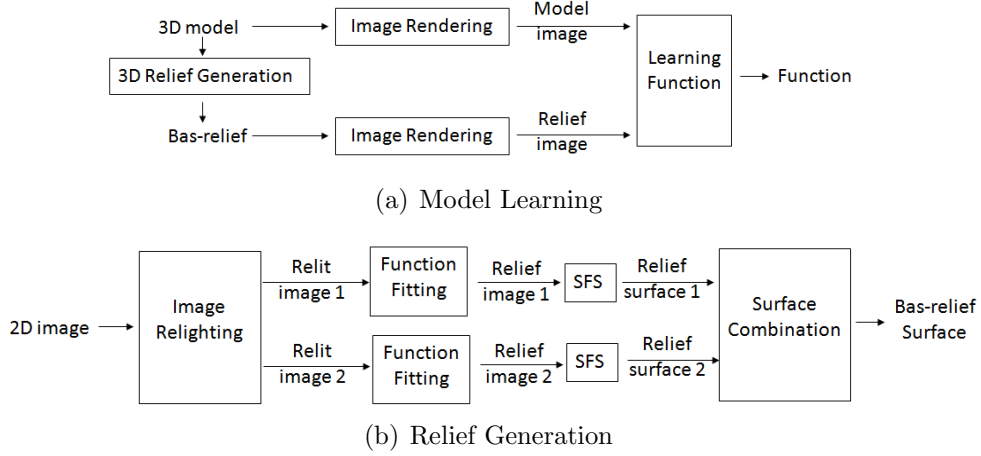


Figure 1: The proposed framework

36 this approach because the results would be dependent on any deficiencies in  
 37 the chosen bas-relief production algorithm. Instead, we take an alternative  
 38 path: we first generate a new image from the face photograph; this new image  
 39 corresponds to the expected appearance of the bas-relief. We then apply SFS  
 40 to this image to recover the shape of the bas-relief. This potentially allows  
 41 us to base our approach on high-quality hand-crafted bas-reliefs, rather than  
 42 algorithmically generated ones, as we now discuss.

43 Our overall framework has two components, shown in Figure 1. First,  
 44 an offline process is used to learn the relationship between an image of a  
 45 3D human face and an image of a corresponding 3D bas-relief of that face.  
 46 This is done by taking one or more 3D face models, and processing them  
 47 using any existing bas-relief generation algorithm to produce corresponding  
 48 3D bas-reliefs. Each original 3D model and corresponding bas-relief are then  
 49 rendered to give 2D images, using one or more lighting conditions. A learning  
 50 algorithm is used to model the relationship between the pixel values in these  
 51 images. While here we use an existing 3D bas-relief generation algorithm  
 52 for simplicity, an alternative would be to learn the relationship using pho-  
 53 tographs of human faces and handcrafted bas-reliefs of those faces derived  
 54 from those photographs. This would avoid any deficiencies in existing bas-  
 55 relief generation algorithms (but would also necessitate careful registration  
 56 of reliefs and photographs).

57 Once we have learnt the model between 2D face images, and 2D face

bas-relief images, we can input a new face image, and apply the model to determine what a corresponding bas-relief model should look like. We then apply SFS to recover the bas-relief surface from the generated bas-relief image. In practice, we find that if we re-light the input image from several new directions [12], giving multiple versions of the input image, and use each to determine a bas-relief, these can be combined into a more satisfactory final bas-relief.

In the following, Section 2 reviews related work on bas-relief generation and shape from shading. Sections 3, 4, and 5 give detailed descriptions of the model building step, bas-relief image generation, and shape from shading. Section 6 describes how multiple renderings may be combined to give a final bas-relief surface. Section 7 presents examples, while Section 8 considers several alternative strategies in our methods. Section 9 gives conclusions and discusses possible improvements.

## 2. Related Work

The earliest attempt to generate bas-reliefs by computer was given in [1]. The authors summarized various basic attributes of artistic bas-reliefs, in particular noting that more distant objects undergo greater depth compression than nearer ones. Based on this finding, the authors applied a standard perspective transformation to the height fields of a 3D scene. Although the results generally adhered to the principles of creating bas-relief, the results only weakly preserved detailed features.

More recent work [2, 4, 3] was inspired by techniques used in high dynamic range (HDR) imaging, where a wide range of intensities is compressed to use a lower intensity range in a way that retains important visual features. In relief processing, depths replace intensities. The method in [4] performs depth compression in the gradient domain, using a non-linear scaling [13] of gradient magnitudes; the aim is to preserve small gradients while attenuating large ones. The approaches in [2] and [3] both make use of unsharp masking to emphasize salient features, before using linear scaling for compression. The former works in differential coordinates, while the latter works in the gradient domain. The results in [3] were improved in [14] by replacing linear scaling with non-linear scaling techniques during compression. Further work of a similar kind [6] also applies non-linear scaling, but uses bilateral filtering to decompose the gradient into coarse and fine components, enabling careful manipulation of detail.

94 A different kind of approach is based on the concept of adaptive histogram  
95 equalization from image processing [5]; depth compression works directly on  
96 the height field. The authors demonstrate good results for various scenes  
97 and objects, including human faces, and we use it as a basis for our learning  
98 process.

99 The above methods start with a *depth-map* of a 3D scene, and selectively  
100 compress depths to create the bas-relief surface. Two recent papers [7, 8]  
101 use *images* as input. A two-level (low frequency component and high fre-  
102 quency detail) approach is given in [8] to restore brick and stone reliefs from  
103 images taken as rubbings. The authors have also applied their approach to  
104 photographs, but, as they note, it is only suitable for objects made of homoge-  
105 neous materials with relatively little texture and low albedo. An experiment  
106 on a photograph of Picasso showed that the approach provided poor results  
107 for portrait photographs.

108 More pertinent to our work is [7], which aims to create relief surfaces that  
109 approximate desired images under known directional lighting. The authors  
110 first adjust the input images to match their average radiance to that of a relief  
111 plane. They then apply a modified SFS method with height constraints to  
112 this adjusted image to create the relief surface. The authors note that the  
113 integrability constraint enforced by SFS constrains the radiance for each  
114 element of a recovered surface. To use this observation, they associate each  
115 pixel with not just one, but several, surface elements. Unfortunately, the  
116 increased numbers of degrees of freedom also increases the sensitivity of the  
117 generated bas-relief surfaces to changes in viewing direction and illumination.

118 An important observation that we have made is that images of real bas-  
119 reliefs, such as heads on coins, *do not* approximate images of the correspond-  
120 ing 3D objects (photographs of heads). Instead, they *enhance* the salient  
121 features. Thus, we do not follow the aims of [7], but instead try to make bas-  
122 relief surfaces with the same appearance as bas-reliefs created by an artist.  
123 Trying to approximate an original photograph is an unrealistic goal given  
124 that the bas-relief surface must be relatively flat. This different emphasis of  
125 approach has a further advantage that the results are not strongly view de-  
126 pendent, and the global geometric nature of each generated bas-relief surface  
127 is consistent with human perception, giving them a stable appearance under  
128 changes of viewing direction and illumination.

129 Our work employs existing SFS techniques, which recover shape from in-  
130 tensity variation in an image. A survey of early SFS work can be found in [9].  
131 Assuming Lambertian reflectance and a known directional light source, Horn

132 and Brooks [15] gave a variational approach to solve the SFS problem. The  
 133 energy to be minimised comprises a brightness constraint and a quadratic  
 134 regularizing term enforcing surface smoothness. However, this method in-  
 135 volves the choice of a Lagrange multiplier, and the results tend to be over-  
 136 smoothed. To overcome these deficiencies, Worthington and Hancock [10]  
 137 proposed a geometric SFS framework which strictly satisfies the brightness  
 138 constraint at every pixel: surface normals are forced to lie on their irradiance  
 139 cones during each iterative update. The same authors have also given sev-  
 140 eral robust regularizers with better smoothing behaviour than the quadratic  
 141 one [16]. Huang and Smith [11] gave a structure-preserving regularization  
 142 constraint, which allows smoothing to be performed locally, dependent on  
 143 the intensities in a local area. We adopt the last method, as it is particularly  
 144 suited to our requirement to preserve salient facial features.

### 145 3. Mapping face images to face bas-relief images

146 As shown in Figure 1, the first step of our framework is to learn the  
 147 relationship between a 2D frontal image (photograph) of a human face and  
 148 a 2D image of a corresponding bas-relief of the same face. The idea is that  
 149 if we know the mapping, we can generate bas-relief images from *new* input  
 150 face images without requiring corresponding 3D models.

151 Initially, we tried an alternative approach (with similar goals to [7]): to  
 152 use the 2D frontal image as a basis for *directly* producing a relief using shape-  
 153 from-shading, with extra constraints to enforce the result to have very low  
 154 height: the aim was to produce a relief which *looks as similar as possible* to  
 155 the input face. It soon became obvious that this does not give satisfactory re-  
 156 sults. On analysing images of artistic bas-reliefs, while they are recognisably  
 157 related to images of the original object, they are also quite clearly different  
 158 from them. Figure 2 shows an example of a bas-relief generated using an ex-  
 159 isting 3D bas-relief generation method [5], clearly demonstrating this point.

160  
 161 We thus turned to understanding and modeling the mapping between  
 162 intensities in images of faces and images of corresponding bas-reliefs. It soon  
 163 became clear that a simple function is not adequate for this purpose. Some  
 164 explicit image processing methods, such as image embossing, can produce an  
 165 image with a bas-relief-like effect. However, these methods usually change  
 166 the reflectance properties of the surface, and the lighting conditions in the  
 167 original image, which increases the difficulty of applying shape-from-shading

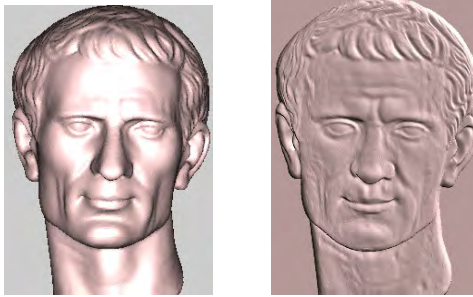


Figure 2: Two images rendered under the same conditions: a 3D model, and a bas-relief generated from it using the method in [5]. Note that these images are very different.

168 in the subsequent steps of our process. Instead, then, we take a different  
 169 strategy, and learn the mapping by training a feedforward network.

170 For training, computer generated 2D frontal images of a 3D face model  
 171 and a corresponding 3D bas-relief model are produced, using the same ren-  
 172 dering setup—the same reflectance model and lighting conditions. We make  
 173 use of this consistency of rendering during the shape from shading step. We  
 174 take the 3D face models as given; during the learning process, to generate  
 175 corresponding bas-reliefs, we use an existing algorithm chosen for its good  
 176 performance on faces [5]. (As noted, better results are likely to be obtained  
 177 using high-quality bas-relief models produced by a sculptor.) We also use a  
 178 saliency map to guide the selection of the training data, so that the more  
 179 salient areas are more likely to be selected during training (and hence better  
 180 modelled). We now give further details.

### 181 3.1. Generating Bas-reliefs for Training

182 To learn the mapping from images of faces to images of bas-reliefs of  
 183 faces, we need corresponding pairs of images. Given one or more 3D face  
 184 models, we need to generate corresponding 3D bas reliefs. We do so using  
 185 Sun’s method [5], which we briefly summarise. Starting from a height map  
 186 of the face (i.e. a range image), it performs histogram equalization of heights  
 187 within a local neighborhood for each point. Two modifications are applied  
 188 to this local histogram equalization. First, the calculation of the histogram  
 189 is weighted by the gradient magnitude after applying a non-linear transfor-  
 190 mation, in order to preserve small shape details. The second modification  
 191 applies an iterative clipping and redistribution procedure to the local his-  
 192 tograms, limiting their content. This prevents too many counts in any one



193 histogram bin, which would result in shape distortion and increased noise.  
 194 A scaling factor  $l$  controls this limit for each bin’s content. To generate the  
 195 final bas-relief surface, the method processes the input height maps using sev-  
 196 eral different neighborhood sizes, and averages the results. Figure 2 shows  
 197 a scanned head of Julius Caesar and the final bas-relief produced using the  
 198 method.

### 199 3.2. Saliency Map Calculation

200 When producing a bas-relief, it is more important to preserve details in  
 201 some areas of the face than others. We define and use a saliency map for  
 202 this purpose. It is used to guide the learning process so that more salient  
 203 areas are more likely to be selected during training. It is also used again later  
 204 in the shape-from-shading process in order to preserve salient facial features  
 205 (see Section 5).

206 The saliency map is computed from the input image; during training  
 207 we also determine saliency maps for the training images. Photographs of  
 208 faces often contain noise, partly due to data acquisition errors, but also both  
 209 because of skin blemishes—small local changes in skin colour not due to a  
 210 change in surface shape. Images of faces generated from 3D mesh models  
 211 may also contain systematic noise due to low mesh resolution. Thus, before  
 212 calculating the saliency map, we use bilateral filtering [17] to smooth the  
 213 image while still preserving the shapes of features.

214 From this bilaterally-filtered image  $I$ , we calculate the image gradient  
 215 magnitude:

$$g(x, y) = \sqrt{\left(\frac{\partial I}{\partial x}\right)^2 + \left(\frac{\partial I}{\partial y}\right)^2}. \quad (1)$$

216 Next, we apply histogram equalization to  $g$  to enhance contrast. The same  
 217 clipping and redistributing procedure described in [5] is also applied to this  
 218 histogram, again using the scaling factor  $l$  to control the level of detail  
 219 retained—retaining too much detail also retains noise. A final, smoothed,  
 220 saliency map is found by applying an averaging filter with a circular neigh-  
 221 bourhood to the result.

222 Examples of saliency maps calculated from images rendered using mesh  
 223 models, and from photographs, are shown in Figure 3; they have resolutions  
 224 of  $596 \times 852$  and  $701 \times 841$  respectively. We use 256 equal-sized bins during  
 225 histogram equalization, and a radius of 3 for the circular averaging filter.  
 226 Results are shown in Figure 3 for varying scaling factors  $l$ ; the saliency maps



(a) saliency maps of a image generated from Julius Caesar model



(b) saliency maps of a real-world image

Figure 3: Examples of saliency maps. Left to right: original images, and saliency maps with  $l = 1, 4, 8, 16, 32$  respectively.

bring out more detail with increasing  $l$ . A reasonable balance between feature  
 details and noise occurs when  $l = 8$ .

### 3.3. Feedforward Network Training

Given a 3D face model and a corresponding (algorithmically generated) bas-relief surface, we now compute an image of each in the same position, using the same lighting conditions and reflectance models. We assume that the intensity of each pixel in the bas-relief image is determined by the intensities in a local neighborhood around the same pixel in the corresponding 3D model image. To learn the relationship between these local neighborhoods and the bas-relief pixel values, we use a feedforward neural network [18] for its simplicity. Other neural networks or learning algorithms could also be used.

In our experiments, we used a 3D model of Julius Caesar and a corresponding generated bas-relief (as shown in section 3.1) to generate the training model images and bas-relief images. We generated two pairs of corresponding training images using Lambertian reflectance and parallel lighting, from lighting directions,  $(1, 1, 1)$  and  $(-1, 1, 1)$ , respectively (with  $z$  towards the model), as shown in Figure 4. For each pair of training images, our feedforward network has one hidden layer with 30 neurons. Each network is



Figure 4: Model images and corresponding bas-relief images used for training. Left pair: light direction  $(1, 1, 1)$ , right pair: light direction  $(-1, 1, 1)$ .

246 trained for up to 1000 epochs and to a mean-square error goal of 0.001. Once  
 247 the error goal is reached, a cross-validation technique is used to determine  
 248 the performance and decide whether to stop training.

#### 249 4. Generating Bas-relief Images

250 Having learnt a mapping from a face image to a bas-relief image, we can  
 251 apply it to new images of faces to generate corresponding bas-relief images.  
 252 However, the images used for training are illuminated under specific lighting  
 253 conditions. Given a new image, for the learnt mapping to be applicable, it  
 254 should be illuminated from the same lighting direction as the training images.  
 255 Various methods exist in the literature which take an image under one set  
 256 of illumination conditions, and re-light it to produce a corresponding image  
 257 under different illumination conditions. We make use of the quotient image  
 258 technique [12] for this purpose.

##### 259 4.1. Image Relighting

260 Three images of the same object under linearly independent light sources  
 261 are sufficient to generate the image space resulting from varying lighting  
 262 directions [19, 20]. The basic idea of the quotient image technique is to  
 263 apply the image space generated from one object to other objects of the  
 264 same kind. The key is to find the quotient image, which is defined as the  
 265 quotient between the objects' albedos. The quotient image is independent of  
 266 illumination, and once it has been determined, the whole image space of the  
 267 new object can be generated from three images of the base object. In [12],  
 268 the authors show how to obtain the quotient image  $Q_y$  given an image  $y_s$  of



(a) Azimuth angle:  $-10^\circ$ , elevation angle:  $-20^\circ$



(b) Azimuth angle:  $-35^\circ$ , elevation angle:  $+15^\circ$



(c) Azimuth angle:  $+35^\circ$ , elevation angle:  $+15^\circ$

Figure 5: Bootstrap set for image relighting.

object  $y$  under a certain light source  $s$ , based on a bootstrap set of training objects  $A_1, \dots, A_N$ . Each  $A_i$  is a matrix whose columns are the three images of a base object  $a_i$ . The use of a bootstrap set instead of a single object allows for variation of albedos. The albedos of the  $N$  training objects are expected to span the albedo of the novel object. Increasing  $N$  in principle gives more freedom to represent novel objects, although experiments in [12] show little difference as  $N$  varies from 2 to 10.

In our experiments, we used a bootstrap set of images of 8 faces from Yale Face Database B [21]. The three images of each face are all frontal, being illuminated from three lighting directions with azimuth and elevation angles of  $(-10^\circ, -20^\circ)$ ,  $(-35^\circ, +15^\circ)$ , and  $(+35^\circ, +15^\circ)$  respectively. The images are coarsely aligned using the tip of the nose and the centers of the eyes. The aligned bootstrap set is shown in Figure 5.

Figure 6 shows examples of applying image relighting using this training data. Two images of the same person are shown under different lighting. Apart from shadows, the quotient images are quite similar, and approximately invariant to changes in light source as hoped. The quotient image technique unfortunately cannot take shadows into account. Relighting images without shadows produces results with a realistic appearance (top row,



Figure 6: Image relighting results, for 2 images of the same person taken under different lighting. Left to right: original image, quotient image, and images relit from directions  $(1, 1, 1)$  and  $(-1, 1, 1)$ .

Figure 6). Due to the simple coarse alignment used, some minor artifacts can be seen in the relit images around the eyes and hair. This could be improved by applying a more sophisticated pointwise alignment method. We return to the problem of shadows later.

#### 4.2. Generating the Bas-relief Images

We are now ready to generate the bas-relief image from the input face image. We first relight it from each of the same lighting directions as the training images, using the quotient image technique. Next, the original image and relit images are scaled, according to the distance between the eyes, to be a similar size to the training images. A saliency map is then calculated from the resized original image, for use later. Next, we apply the learnt feedforward networks to the relit images, to get the pixel values in the bas-relief images from pixel neighborhoods in the relit images.

Examples of generated bas-relief images are shown in Figure 7 (The intensity of the relief images are linearly stretched for showing purpose.). Salient facial features are preserved in the generated images, giving these images recognizable bas-relief appearance. The lighting directions used in the relit model images are also evident in the bas-relief images, and are utilized directly in the following shape-from-shading step.

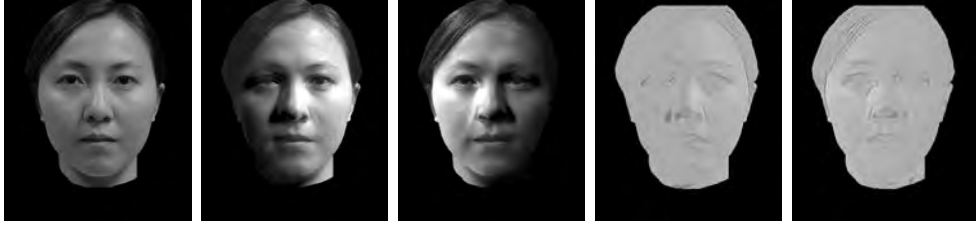


Figure 7: A generated bas-relief image. Left to right: original image, two relit images, and corresponding bas-relief images.

## 5. Finding the Relief using Shape-from-shading

We now apply shape-from-shading (SFS) to each constructed relief image, to determine the geometry of the relief surface. SFS recovers shape from variation of intensities in the image. Most popular SFS methods solve the problem by minimizing an energy function, which usually includes an intensity constraint (that the surface orientation should lead to the observed intensity) and a regularizing term (enforcing surface smoothness). A basic energy function for Lambertian surfaces is given in [15]:

$$I = \int \int \underbrace{(E(x, y) - \mathbf{n}(x, y) \cdot \mathbf{s})^2}_{\text{Brightness Error}} + \lambda \underbrace{\left( \left| \frac{\partial \mathbf{n}(x, y)}{\partial x} \right|^2 + \left| \frac{\partial \mathbf{n}(x, y)}{\partial y} \right|^2 \right)}_{\text{Regularizing Term}} dx dy, \quad (2)$$

where  $E(x, y)$  and  $\mathbf{n}(x, y)$  are respectively the image intensity and the surface normal at pixel location  $(x, y)$ ,  $\mathbf{s}$  is the direction of the light source, and  $\lambda$  balances intensity fidelity against surface smoothness. In practice, surfaces recovered using this formulation are often over-smoothed.

Our SFS method improves upon this formulation in two ways. First, we satisfy intensity closeness as a hard constraint using the method of Worthington and Hancock [10]. The aim is to preserve the appearance of the image, which is important in our application. Secondly, we use a modified version of Huang and Smith's [11] structure-preserving regularization constraint, which helps to preserve salient facial features. Our SFS method is iterative. In each iteration, the surface normals are updated to first satisfy the regularizing term, and secondly to satisfy the brightness constraint. Finally, we use the algorithm of Frankot and Chellappa [22] to integrate the field of recovered surface normals to generate the bas-relief surface. We now

329 give further details.

### 330 5.1. Brightness Constraint

331 For Lambertian surfaces, satisfying the intensity closeness as a hard con-  
332 straint is equivalent [10] to enforcing

$$\int \int (E(x, y) - \mathbf{n}(x, y) \cdot \mathbf{s})^2 dx dy = 0. \quad (3)$$

333 This causes the surface normal at pixel  $(x, y)$  to lie on a cone whose axis is  
334 in the light source direction  $\mathbf{s}$  and whose opening angle is  $\alpha = \cos^{-1} E(x, y)$ .  
335 During each iteration of SFS, after updating the surface normals according to  
336 the regularizing term, the updated surface normals usually do not lie on the  
337 cone. Then, we need to rotate them back to their closest on-cone positions  
338 to enforce the brightness constraint.

### 339 5.2. Regularization Constraint

340 Enforcing the regularizing constraint in Equation (2) during each iteration  
341 of SFS can be done by updating the surface normals using

$$\mathbf{n}^{(t+1)}(x, y) = \frac{1}{4} \sum_{(i,j) \in \Omega(x,y)} \mathbf{n}^{(t)}(i, j), \quad (4)$$

342 where  $\Omega(x, y) = \{(x+1, y), (x-1, y), (x, y+1), (x, y-1)\}$  is the local neigh-  
343 borhood. The structure preserving regularization constraints in [11] modify  
344 Equation (4) by introducing a weighting scheme. The idea is that adjacent  
345 pixels with closer intensities are more likely to have similar surface normal  
346 directions. Instead, surface normals are updated using

$$\mathbf{n}^{(t+1)}(x, y) = \frac{\sum_{(i,j) \in \Omega(x,y)} W(i, j) \mathbf{n}^{(t)}(i, j)}{\left\| \sum_{(i,j) \in \Omega(x,y)} W(i, j) \mathbf{n}^{(t)}(i, j) \right\|}, \quad (5)$$

347 where  $W(i, j)$  is a normalized measure of the intensity similarity between  
348 pixel  $(i, j)$  and the current pixel  $(x, y)$ . It provides surface smoothness when  
349 adjacent pixels have similar intensities, but smoothing is reduced when there  
350 are large differences in intensities. During each SFS iteration, this weighted  
351 updating of surface normals is iterated until convergence (the angular dif-  
352 ference between  $\mathbf{n}^{(t)}$  and  $\mathbf{n}^{(t+1)}$  is less than a predefined  $\xi$ ) or a predefined  
353 maximum number of iterations (set to 200 in our experiments).



Figure 8: Surface normal adjustment. Left: result before adjustment; right: after adjustment.

Our variant of this approach replaces the weight  $W(i, j)$  in Equation (5) with the saliency value at location  $(i, j)$ . Thus, updated surface normals are more determined by positions with high saliency values than with low saliency values, which helps to preserve salient facial features.

### 5.3. Surface Normal Adjustment

After the surface normals have been recovered from the image by iteratively satisfying the above regularization constraint and brightness constraint, we apply a further step of postprocessing. Suppose at position  $(x, y)$ , the angle between the recovered surface normal and the light source direction is  $\theta(x, y) = \cos^{-1}(\mathbf{n}(x, y) \cdot \mathbf{s})$ , and the saliency value normalized to  $[0, 1]$  is  $w(x, y)$ . Then, we adjust the angle to be

$$\hat{\theta}(x, y) = w(x, y)\theta(x, y). \quad (6)$$

Together with the light source direction  $\mathbf{s}$ , this defines a new cone at position  $(x, y)$ . We rotate  $\mathbf{n}(x, y)$  to its closest on-cone position. Adjusted in this way, we reduce differences of surface normals in areas with low saliency values, while increasing differences between areas with low saliency values and areas with high saliency values. As a result, we achieve a smoother surface with more prominent features. An example of relief surfaces generated with and without this adjustment step are shown in Figure 8.

## 6. Combination of Relief Surfaces

Our whole process (training, generating bas-relief images, and shape-from-shading) is based on predefined lighting directions. We use lighting from above (as this is natural), and to one side, to emphasize facial features.



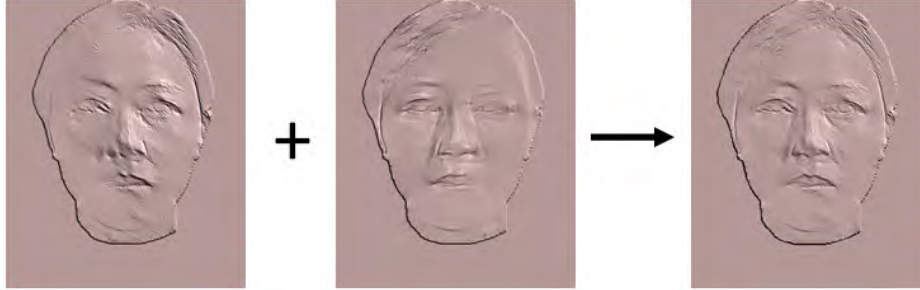


Figure 9: Combination of left- and right-illuminated relief surfaces.

376 The drawback is that features are revealed in an uneven way. Features inside  
 377 shadows, and those facing the light, are hard to see, while those in other  
 378 areas are revealed much better. We overcome this difficulty by repeating the  
 379 whole model building process *twice* using two symmetric lighting directions  
 380 from upper right  $(1, 1, 1)$  and upper left  $(-1, 1, 1)$ . *Two* bas-relief surfaces are  
 381 generated, and we use the average surface as the final output (alternatives to  
 382 this approach are discussed further later). Figure 9 shows an example of the  
 383 two bas-relief surfaces generated from the same original photograph, and their  
 384 average. These two surfaces were recovered from the two generated bas-relief  
 385 images in Figure 7. The average surface combines features independently  
 386 revealed by the two surfaces, and further smooths out noise.

## 387 7. Experimental Results and Discussion

388 We now present various results obtained using our method. Various issues  
 389 should be considered when deciding if the results are satisfactory. The first  
 390 is whether the salient features are distinct and well-preserved, making the  
 391 face recognisable, and can be best assessed by visual inspection of the results.  
 392 The second is whether the geometry of the generated bas-relief is appropri-  
 393 ate, so that the relief’s appearance is stable under changes of viewing and  
 394 illuminating directions. We show height maps of the generated bas-reliefs to  
 395 reveal their overall geometries. (As shape-from-shading is an ill-posed prob-  
 396 lem, it is possible to recover a shape which looks correct from the original  
 397 viewing direction, but is clearly the wrong shape when viewed from another  
 398 direction—for example, it is well-known that convexity and concavity can be  
 399 reversed [23]). A third issue is that the results should not contain unwanted  
 400 noise.

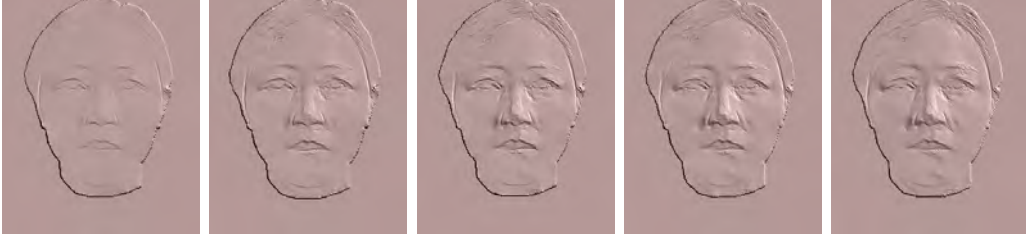


Figure 10: Bas-relief surfaces generated using different saliency scaling factors  $l$ . Left to right: surfaces using  $l = 1, 4, 8, 16$ , and  $32$ .

401 In the first experiment, we examine how varying the scaling factor  $l$   
 402 in the saliency map calculation affects the amount of detail in the gener-  
 403 ated bas-relief surfaces. Figure 10 shows bas-relief surfaces generated using  
 404  $l = 1, 4, 8, 16, 32$ ; as  $l$  increases, the surfaces show more detail, but also  
 405 more noise. When  $l = 1$ , salient features are not clearly revealed. For  
 406  $l = 4, 8, 16, 32$ , the differences between the surfaces are more subtle. A suit-  
 407 able compromise seems to be  $l = 8$ , which we used in other experiments.  
 408 We note that real reliefs on coins often prefer smoothness of the relief at the  
 409 expense of fine detail.

410 In the second experiment, we assess the overall geometry of the generated  
 411 bas-relief surfaces, and their appearance under different lighting directions.  
 412 Figure 11 shows generated bas-relief surfaces using  $l = 8$ , together with  
 413 their height fields which help to reveal their overall geometry. We also give  
 414 views of the surfaces when illuminated under four different lighting directions:  
 415  $(1, 1, 1)$ ,  $(-1, 1, 1)$ ,  $(-1, -1, 1)$ , and  $(1, -1, 1)$ . We can see that the generated  
 416 bas-relief surfaces are smooth and maintain the salient facial features in each  
 417 case. The overall geometry of each bas-relief is globally of the desired shape,  
 418 which ensures that its appearance is as expected under changes of viewing  
 419 and lighting directions. One drawback is that the lips are surprisingly and  
 420 somewhat undesirably lower than the surrounding area. This is because  
 421 these areas are typically dark in the face, but in the SFS process, we have  
 422 assumed constant albedo without taking such coloration into account. The  
 423 SFS method can only produce the coloration by a geometric adjustment, and  
 424 in doing so, the dark area poses the concave / convex ambiguity problem. On  
 425 the other hand, the same effect is beneficial elsewhere in the image: eyebrows  
 426 in particular are clearly visible in the result, even though geometrically they  
 427 are close to the underlying face. A possible improvement could be obtained

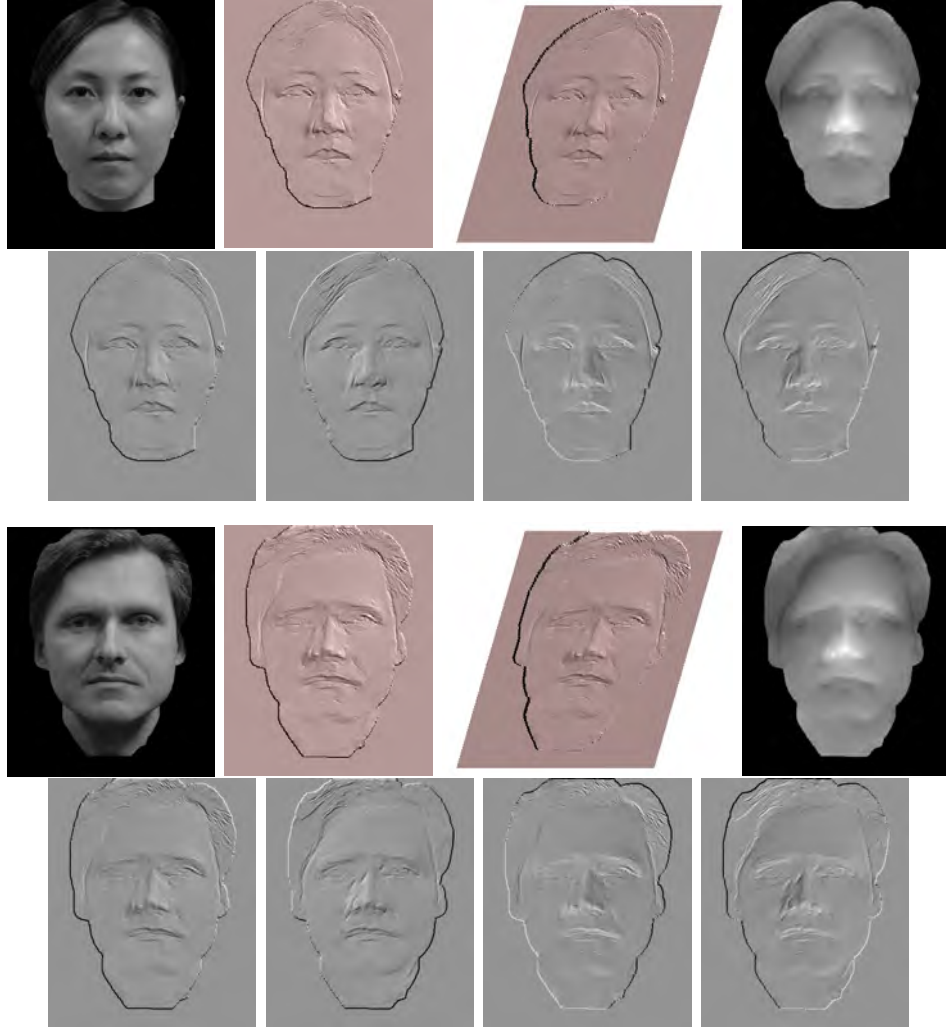


Figure 11: Output bas-relief surfaces. Rows 1, 3: original photograph, relief surface viewed from 2 angles, and the corresponding height fields. Rows 2, 4: views of the relief surface using four different lighting directions:  $(1, 1, 1)$ ,  $(-1, 1, 1)$ ,  $(-1, -1, 1)$ , and  $(1, -1, 1)$ .

428 by taking facial albedo into account during SFS, at least for the lips.

429 Further results are shown in Figure 12, using photographs captured un-  
 430 der ambient (rather than directional) light. Figure 13 shows results from  
 431 public domain photographs of various famous people. Faces were cropped  
 432 from backgrounds manually. In each case, reasonable bas-relief surfaces were  
 433 produced. One limitation is that teeth (last row in Figure 12 and Figure 13)

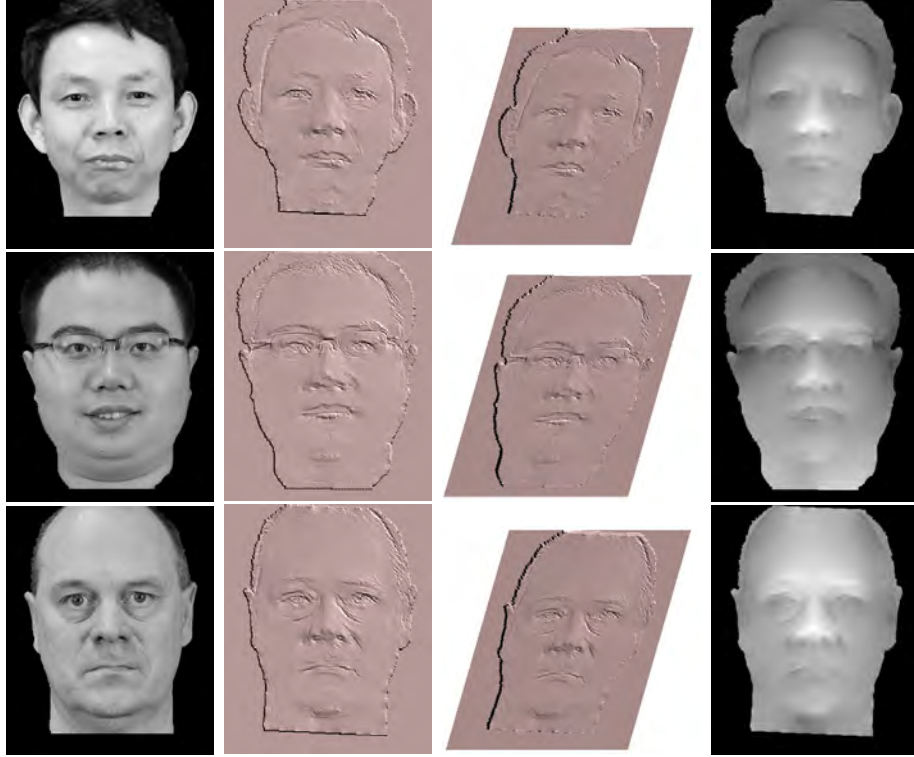


Figure 12: Further reliefs produced from photographs under ambient light.

434 and extensive hair (first row in Figure 13) are not handled well, because they  
 435 are not well represented in the relief training data and bootstrap images for  
 436 relighting. A further possible improvement would be to enlarge the training  
 437 and bootstrap sets to include various facial albedos and expressions.

438 Finally, we applied our method to a photograph of a non-frontal face—  
 439 see Figure 14. The generated bas-relief surface reveals the general shape of  
 440 the face and maintains the prominent features. However, there are artifacts  
 441 around the eyes and mouth. Figure 14 makes it clear that the artifacts are  
 442 introduced during image relighting. The bootstrap set used for image relight-  
 443 ing was entirely composed of frontal faces. Our simple alignment procedure  
 444 did not do a good job of aligning this image to the bootstrap set, causing the  
 445 artifacts observed. Better fine alignment, or a point-to-point correspondence  
 446 method is likely to improve the results.

447 Our prototype implementation using MATLAB 7.9.0. Approximate com-  
 448 putational times taken by each step of our method are shown in Table 7, for

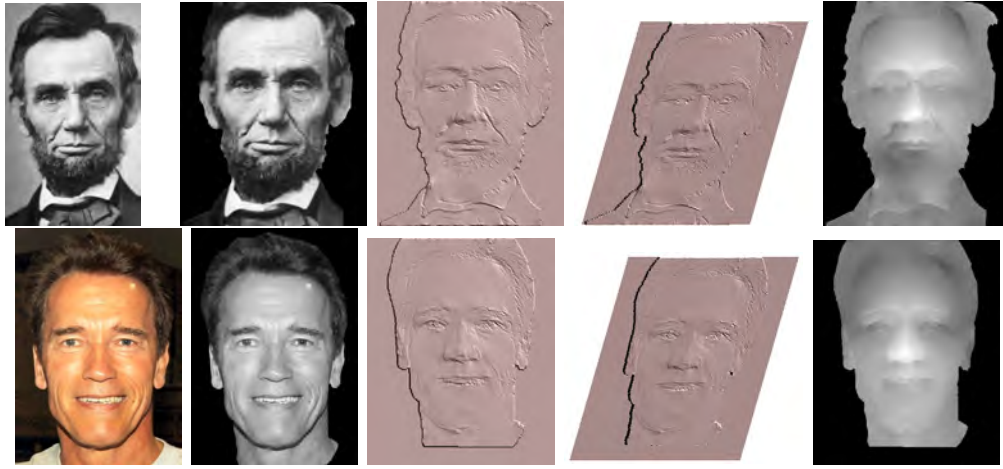


Figure 13: Reliefs of famous people. The first two columns show the input photograph, and the aligned grayscale image derived from it.

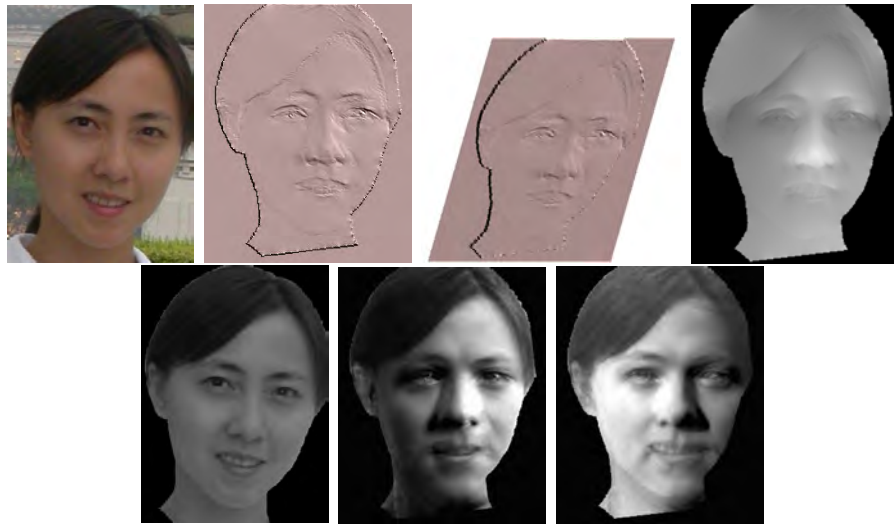


Figure 14: Results on photographs of a non-frontal face. Top: photograph and relief, bottom: relit images.

449 images of size  $701 \times 841$ . Neural network training step took the longest time  
 450 (3 hours) but needs doing only once. Given a new photograph, there are five  
 451 steps to get the final bas-relief surface, taking about 5 minutes in total; this  
 452 could probably be reduced by a high-level language implementation. Note  
 453 that the time for image relighting includes the time for manually marking

454 landmarks to perform coarse alignment.

Table 1: Approximate timings.

Step	Time
Neural Network Training	3 hours
Saliency Map Calculation	16 seconds
Image Relighting	16 seconds
Generating Relief Images	8 seconds
Shape from Shading	4 minutes
Surface Combination	0.05 seconds

## 455 8. Variants

456 We finish by considering various alternative strategies we have investi-  
457 gated, but rejected.

458 First, in the network training process, we train a single neural network  
459 from the training data. However, to generate a plausible bas-relief surface,  
460 areas with low saliency and high saliency should be compressed in different  
461 ways. *Identical* local neighborhoods in the input image may lead to pixels  
462 with *different* values in the relief image, in places of different saliency. To  
463 allow for this, we considered an alternative strategy during neural network  
464 training. We divided the input image into several bands according to the  
465 saliency value of each pixel, and trained a separate network for each band.  
466 We perform experiments using 2, 3, 5, and 10 bands, and compare the results  
467 with using a single band (as described earlier). The generated bas-relief  
468 images and corresponding bas-relief surfaces are shown in Figure 15. It is  
469 clear that greater intensity variation occurs in the generated bas-relief images  
470 when using more bands, and the salient features are more pronounced than  
471 when using one band. These more strongly emphasized areas protrude more  
472 in the final bas-relief surfaces. However, whether such protruding features  
473 are desired in bas-relief creation remains an open question. We can see no  
474 obvious reason for preferring the results using multiple bands, and indeed,  
475 in places they can look worse—e.g. the hair line looks less natural in these  
476 examples.



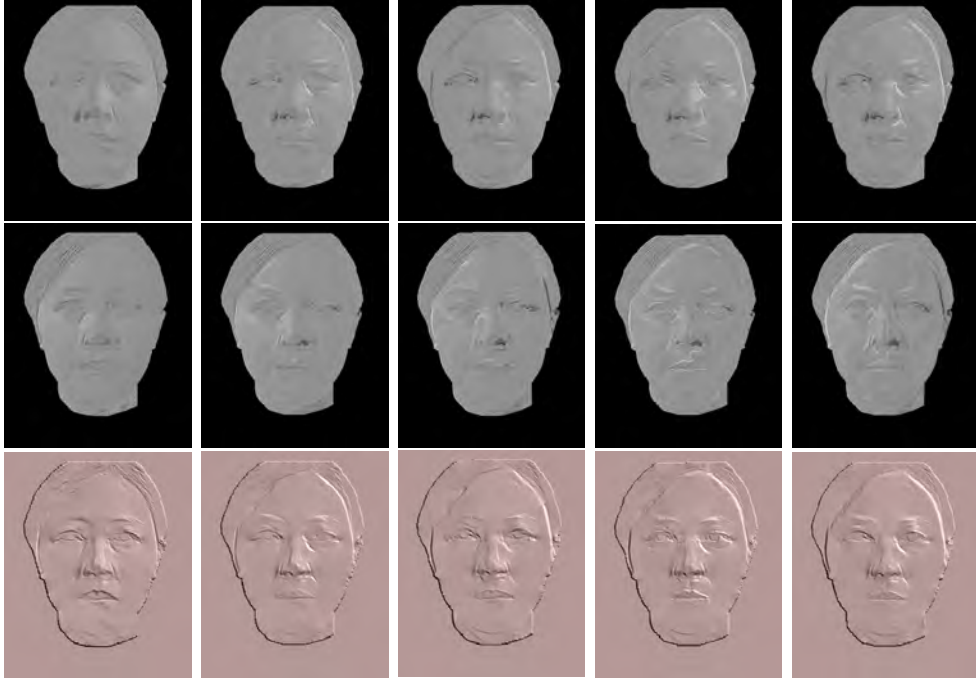


Figure 15: Bas-relief images (with 2 lighting directions) and surfaces generated using 1, 2, 3, 5 and 10 saliency bands.

Secondly, in the surface combination step, we average the two surfaces  $S_1$  and  $S_2$ , which are recovered under two lighting directions, to get the final bas-relief surface. However, as we have noted earlier, each image contains some areas in shadow, or with highlights, which lead to poor shape recovery, and it is plausible that rather than simply *averaging* the two relief surfaces produced, we should use some sort of *selection* procedure to locally choose the good parts from each. Shadows and highlights have intensities far from the mean intensity, so we should preferentially use shape information from the image whose intensity is closest to the mean intensity. Suppose  $I_1$  and  $I_2$  are the two relit images under lighting directions  $(1, 1, 1)$  and  $(-1, 1, 1)$  and  $\bar{I} = (I_1 + I_2)/2$  is the mean intensity value. We compute the absolute difference between the two images and the mean value, i.e.

$$\Delta_1(x, y) = |I_1(x, y) - \bar{I}|, \quad \Delta_2(x, y) = |I_2(x, y) - \bar{I}|. \quad (7)$$

489 Then, we define a combination map

$$M(x, y) = \begin{cases} 1 & \Delta_1 \leq \Delta_2 \\ 0 & \text{otherwise} \end{cases} \quad (8)$$

490 The top left image in Figure 16 illustrates this combination map. An alter-  
491 native, to avoid abrupt transitions is to use a weighted version  $M'$  of  $M$  (see  
492 the bottom left image in Figure 16):

$$M'(x, y) = \frac{\Delta_2(x, y)}{\Delta_1(x, y) + \Delta_2(x, y)}. \quad (9)$$

493 The final bas-relief surface  $S$  is now produced from  $S_1$  and  $S_2$  using the  
494 combination map:

$$S(x, y) = M^*(x, y)S_1(x, y) + (1 - M^*(x, y))S_2(x, y), \quad (10)$$

495 where  $M^*$  is either  $M$  or  $M'$ . The middle column of Figure 16 shows the  
496 combined bas-relief surfaces using combination maps  $M$  (top row) and  $M'$   
497 (bottom row). It is clear that when using combination map  $M$ , there are  
498 discontinuities where the two surfaces meet. Using the weighted combination  
499 map  $M'$  mitigates this problem, but the output surface is still noisy. An  
500 alternative to further avoid this issue is to use the weighted combination  
501 map to take surface normals values from  $S_1$  and  $S_2$ , and integrate them  
502 using the algorithm of Frankot and Chellappa [22]. The bottom right image  
503 in Figure 16 shows the resulting bas-relief surface. Compared to the bas-relief  
504 surface combined using simple averaging (the top right image in Figure 16),  
505 the final bas-relief emphasises features more strongly, but is perhaps less  
506 aesthetically pleasing as defects are also more obvious. This last approach is  
507 also somewhat more computationally expensive.

## 508 9. Conclusions and future work

509 Bas-reliefs of human faces are of particular interest in art and design. We  
510 have given a method, based on neural networks, image relighting, and shape-  
511 from-shading techniques to automatically generate bas-reliefs from frontal  
512 photographs of faces. Experimental results show that our method is capable  
513 of generating reasonable bas-relief surfaces from such photographs, and are  
514 a first step towards automating this process to assist artists.



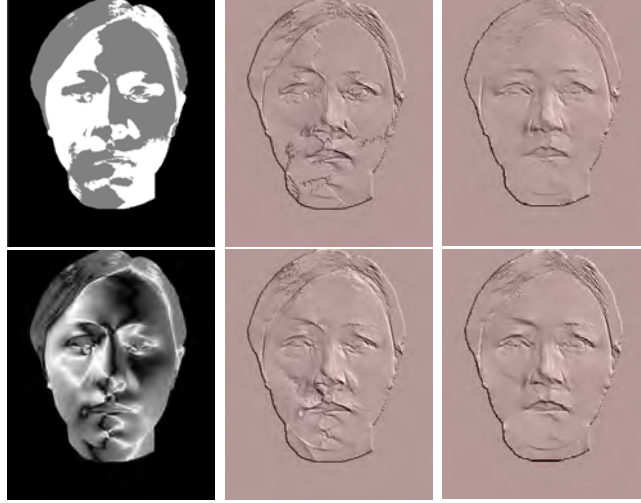


Figure 16: Alternative surface combination methods. Top: 0-1 combination map, relief from 0-1 map, relief using default averaging approach. Bottom: Weighted combination map, relief from weighted map, relief using weighted map to produce normals and integrating.

515 While we have already experimented with some variants of our approach,  
516 there is clearly room for improvement, and we suggest a few avenues that  
517 could improve our method further. In image relighting, the simple coarse  
518 alignment method used results in various artifacts which are visible in the  
519 final output, especially when applying the method to semi-profile faces. Bet-  
520 ter fine alignment, or a more sophisticated point-to-point correspondence  
521 method could reduce this problem. Improvements could be made by tak-  
522 ing into account facial albedo information during the SFS step, and other  
523 reflectance models than the simple Lambertian model used here may also  
524 further improve the results. Clearly, in the function learning process, more  
525 than one training image, and training images from real face models, could  
526 also improve our results. An enlarged bootstrap set in the image relighting  
527 process could better span the space of facial albedos, and as a result, could  
528 also improve the results. Finally, practical applications demand extension of  
529 our method to faces seen in profile, and to a wider class of objects.

## 530 References

- 531 [1] P. Cignoni, C. Montani, R. Scopigno, Computer assisted generation of  
532 bas- and high-reliefs, *Journal of Graphics Tools* 2 (3) (1997) 15–28.
- 533 [2] W. Song, A. Belyaev, H. Seidel, Automatic generation of bas-reliefs from  
534 3d shapes, in: *Proceedings of IEEE International Conference on Shape  
535 Modeling and Applications*, 2007, pp. 211–214.
- 536 [3] J. Kerber, A. Belyaev, H. Seidel, Feature preserving depth compres-  
537 sion of range images, in: *Proceedings of the 23rd Spring Conference on  
538 Computer Graphics*, 2007, pp. 110–114.
- 539 [4] T. Weyrich, J. Deng, C. Barnes, S. Rusinkiewicz, A. Finkelstein, Digital  
540 bas-relief from 3d scenes, in: *ACM Transactions on Graphics (TOG) -  
541 Proceedings of ACM SIGGRAPH 2007*, Vol. 26, 2007.
- 542 [5] X. Sun, P. L. Rosin, R. R. Martin, F. C. Langbein, Bas-relief generation  
543 using adaptive histogram equalization, *IEEE Transactions on Visualiza-  
544 tion and Computer Graphics* 15 (4) (2009) 642–653.
- 545 [6] J. Kerber, A. Tevs, A. Belyaev, R. Zayer, H.-P. Seidel, Feature sensitive  
546 bas relief generation, in: *Proceedings of IEEE International Conference  
547 on Shape Modeling and Applications (SMI)*, 2009, pp. 148–154.
- 548 [7] M. Alexa, W. Matusik, Reliefs as images, in: *ACM Transactions on  
549 Graphics (TOG) - Proceedings of ACM SIGGRAPH 2010*, Vol. 29, 2010.
- 550 [8] Z. Li, S. Wang, J. Yu, K.-L. Ma, Restoration of brick and stone relief  
551 from single rubbing images, *IEEE Transactions on Visualization and  
552 Computer Graphics*.  
553 URL <http://doi.ieeecomputersociety.org/10.1109/TVCG.2011.26>
- 554 [9] R. Zhang, P.-S. Tsai, J. Cryer, M. Shah, Shape from shading: A survey,  
555 *IEEE Transactions on Pattern Analysis and Machine Intelligence* 21 (8)  
556 (1999) 690–706.
- 557 [10] P. Worthington, E. Hancock, New constraints on data-closeness and  
558 needle map consistency for shape-from-shading, *IEEE Transactions on  
559 Pattern Analysis and Machine Intelligence* 21 (12) (1999) 1250–1267.

- [11] R. Huang, W. Smith, Structure-preserving regularisation constraints for shape-from-shading, in: International Conference on Computer Analysis of Images and Patterns, 2009, pp. 865–872.
- [12] T. Riklin-Raviv, A. Shashua, The quotient image: Class based rendering and recognition with varying illuminations, IEEE Transactions on Pattern Analysis and Machine Intelligence 23 (2) (2001) 129–139.
- [13] R. Fattal, D. Lischinski, M. Werman, Gradient domain high dynamic range compression, ACM Transactions on Graphics 21 (3) (2002) 249–256.
- [14] J. Kerber, Digital art of bas-relief sculpting, Master’s thesis, University of Saarland, Saarbrücken, Germany (2007).
- [15] B. Horn, M. Brooks, The variational approach to shape from shading, Computer Vision, Graphics, and Image Processing 33 (2) (1986) 174–208.
- [16] P. Worthington, E. Hancock, Needle map recovery using robust regularizers, Image and Vision Computing 17 (8) (1999) 545–558.
- [17] C. Tomasi, R. Manduchi, Bilateral filtering for gray and color images, in: In Proceedings of the IEEE International Conference on Computer Vision, 1998.
- [18] T. Fine, Feedforward neural network methodology, Springer Verlag, 1999.
- [19] A. Shashua, Illumination and view position in 3d visual recognition, in: In Proceedings of the fourth annual conference on Advances in Neural Information Processing Systems, 1991, pp. 404–411.
- [20] A. Shashua, On photometric issues in 3d visual recognition from a single 2d image, International Journal of Computer Vision 21 (1997) 99–122.
- [21] A. Georgiades, P. Belhumeur, D. Kriegman, From few to many: Illumination cone models for face recognition under variable lighting and pose, IEEE Transactions on Pattern Analysis and Machine Intelligence 23 (6) (2001) 643–660.

- 591 [22] R. Frankot, R. Chellappa, A method for enforcing integrability in shape  
592 from shading algorithms, IEEE Transactions on Pattern Analysis and  
593 Machine Intelligence 10 (4) (1988) 439–451.
- 594 [23] E. Prados, O. Faugeras, Shape from shading: a well-posed problem?,  
595 in: In Proceedings of IEEE Computer Society Conference on Computer  
596 Vision and Pattern Recognition, Vol. 2, 2005, pp. 870–877.